Progress In Electromagnetics Research M, Vol. 81, 137–147, 2019

Analytical Calculation of Magnetic Field Distribution in the Consequent-Pole Bearingless PM Motor with Rotor Eccentricity

Libing Jing*, Zhangxian Huang, and Jun Gong

Abstract—In this paper, an analytical calculation of the magnetic field in a consequent-pole bearingless permanent magnet (PM) type motor with rotor eccentricity is proposed. The analytical method is based on the resolution of Laplace's and Poisson's equations. Due to the presence of consequent-pole, the general solution of the first-order for the vector potential distribution in the air-gap is presented considering the first harmonic. Here, the magnetic field distributions by the analytical method are compared with those obtained from finite element (FE) analyses. Then, the corresponding performances are quantitatively assessed by the finite-element method.

1. INTRODUCTION

Bearingless motor has been developed rapidly in recent years. In consequent-pole bearingless PM motor, the same polarity PM is along the radial direction. The core between PMs is magnetized to another polarity along the radial direction. The PM pole and rotor pole constitute an alternating distribution. The suspension force of the motor is independent of the rotor position angle. The coupling degree of suspension control and torque control is much lower than that of the traditional permanent magnet motor. The levitation winding of this motor can provide radial electromagnetic forces in place of bearings. It not only has a simple structure and high power factor but also inherits the advantages of no friction, no abrasion, and no lubrication of conventional magnetic suspension motors. So it was used widely in ultra-high speed motors [1]. Compared with conventional bearingless motor, consequent-pole bearingless motor can produce radial electromagnetic force, which is independent of the rotor position [2, 3]. So it can achieve the decoupling characteristics of torque and radial suspension force control [4]. It has more practical advantages in the fields of flywheel energy storage, spindle motors of various high-speed machine tools and sealed pumps, centrifuges, compressors, high-speed micro-hard disk drive devices, etc. It has become one of the most promising schemes to realize bearingless motor technology.

It is important to calculate the air-gap magnetic field and unbalanced magnet pull considering rotor eccentricity for the bearingless motors. The air-gap magnetic field can be evaluated by analytical or numerical techniques like finite elements (FE). FE gives accurate results considering geometric details and nonlinearity of magnetic materials [5, 6]. However, this method is computer time consuming and poorly flexible for the first step of design stage of a motor. Analytical methods are useful tools for first evaluation of motor performances and for design optimization since continuous derivatives issued from the analytical solution are of great importance in most optimization methods.

Kim and Lieu studied the magnetic field of PM motors with rotor eccentricity for both slotless and slotted motors [7, 8]. The perturbation method was proposed to predict air-gap flux density distributions, and the imbalance magnetic force and cogging torque in brushless PM motors were calculated. They also gave the characteristic frequencies of the unbalanced force and cogging torque due

Received 12 March 2019, Accepted 22 May 2019, Scheduled 3 June 2019
* Corresponding author: Libing Jing (jinglibing163@163.com).
The authors are with the College of Electrical Engineering & New Energy, China Three Gorges University, Yichang 443002, China.

to rotor eccentricity [9]. In [10], Rahideh and Korakianitis built upon their previous work and presented the no-load magnetic field distribution of slotless brushless PM machines. Magnetic field was calculated under different magnetization patterns of PM. The line and phase back-EMF waveforms, local traction components, and unbalanced magnetic forces are obtained. Reference [11] presented radial component and tangential component of air-gap flux density in different rotor position considering both rotor eccentricity and stator slots. Reference [12] studied a magnetic field of consequent-pole bearingless PM motor without considering the eccentricity of PM motor. However, these researchers just analyzed magnetic field of PM machines, but did not consider primary harmonic which is brought by eccentricity.

The aim of this paper is to propose an analytical solution of the magnetic field distribution in a consequent-pole bearingless PM motor accounting for rotor eccentricity. The Laplace and Poisson's equations are solved in 2-D polar coordinates. The result is proved by FEM. This work can be used for applications regarding rotor eccentricity of other surface mounted motors and embedded PM motors.

2. ANALYTICAL MODEL AND ASSUMPTIONS

Schematic representation of the studied consequent-pole bearingless PM motor with rotor eccentricity is shown in Fig. 1.

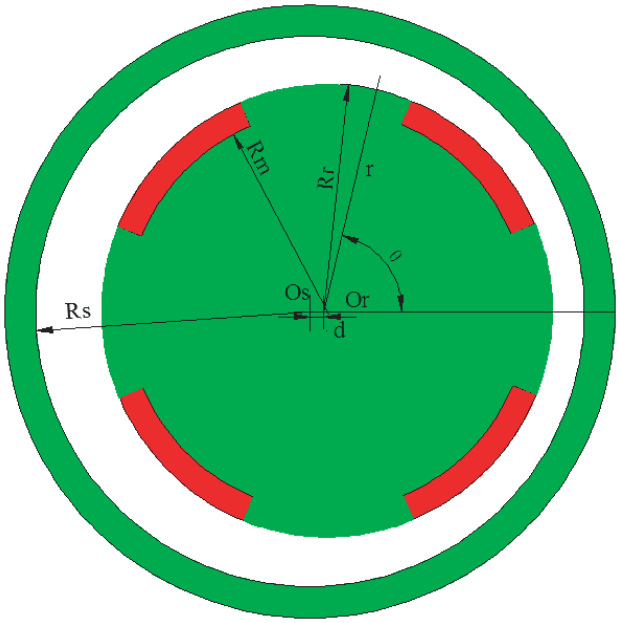

Figure 1. Geometry of the studied motor.

It consists of a p pole-pairs inner rotor, and O_s and O_r are the center of the stator and rotor, respectively. The internal rotor rotates about the axis O_r with the angular velocity of ω. The distance between the two centers is d. The PMs are radially magnetized in the same direction. The geometrical parameters are: R_r is the radius of the rotor, R_m the inner radius of the PM surface, and R_s the radius of the stator. The domain of the magnetic field is divided into two subdomains: one is air-gap subdomain, and the other one is PMs subdomain. The eccentricity ratio (ε) is defined as,

$$\varepsilon = \frac{d}{R_s} \tag{1}$$

Figure 2 is the flowchart of its calculation.

In this paper, some assumptions are adopted as follows:

1) The rotor, stator, and PM surfaces are perfect cylinders;
2) The axes of rotor and stator are parallel;

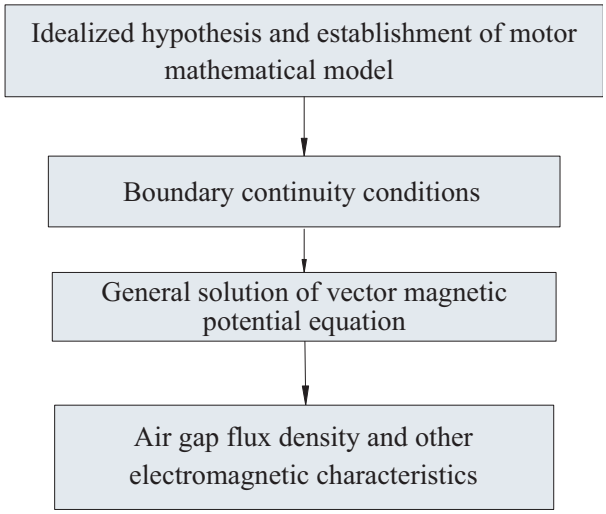

Figure 2. Flow chart.

3) The effects of slotting are neglected;
4) The permeability of the rotor and stator is infinite;
5) Eddy current and saturation effects are neglected;
6) The relative permeability of PM is 1.

In the 2-D coordinate system, the stator circular trajectory can be described as following [13],

$$r = R_s + \varepsilon\delta(\theta) + \mathrm{O}\left(\varepsilon^2\right) \tag{2}$$

As shown in Fig. 1, r can be expressed as follows:

$$r = \sqrt{R_s^2 - (d\sin\theta)^2} - d\cos\theta \tag{3}$$

In the binomial expansion, Eq. (3) can be expressed as

$$r \approx R_s - \frac{1}{2}\frac{d^2}{R_s}\sin^2\theta - d\cos\theta \tag{4}$$

here

$$\delta(\theta) = -\frac{1}{4}d + \frac{1}{4}d\cos 2\theta - R_s\cos\theta \tag{5}$$

The stator boundary can be described by

$$f(r,\theta,\varepsilon) = r - R_s + \frac{1}{4}\varepsilon d - \frac{1}{4}\varepsilon d\cos 2\theta + \varepsilon R_s\cos\theta \tag{6}$$

2.1. Governing Equations and Boundary Conditions

Without any current, the magnetic field intensity vector is curl free. The vector potential is adopted, and the governing equations of the two subdomains are [14];

$$\frac{\partial^2 A_1}{\partial r^2} + \frac{1}{r}\frac{\partial A_1}{\partial r} + \frac{1}{r^2}\frac{\partial^2 A_1}{\partial\theta^2} = 0 \quad for \quad \begin{cases} R_r \le r \le R_s \\ \theta_j \le \theta \le \theta_j + a \end{cases} \tag{7}$$

$$\frac{\partial^2 A_2}{\partial r^2} + \frac{1}{r}\frac{\partial A_2}{\partial r} + \frac{1}{r^2}\frac{\partial^2 A_2}{\partial\theta^2} = -\mu_0\nabla\times\mathbf{M} \quad for \quad \begin{cases} R_m \le r \le R_r \\ \theta_j \le \theta \le \theta_j + a \end{cases} \tag{8}$$

where $\mathbf{M}$ is the magnetization vector, and the radial magnetization is shown in Fig. 3, which can be expressed as,

$$\mathbf{M}(r,\theta) = M_r(\theta)\mathbf{r} = \left[a_0 + \sum_{m=1}^{\infty} M_m \sin\frac{m\pi}{a}\left(\theta - \theta_j\right)\right]\mathbf{r} \tag{9}$$

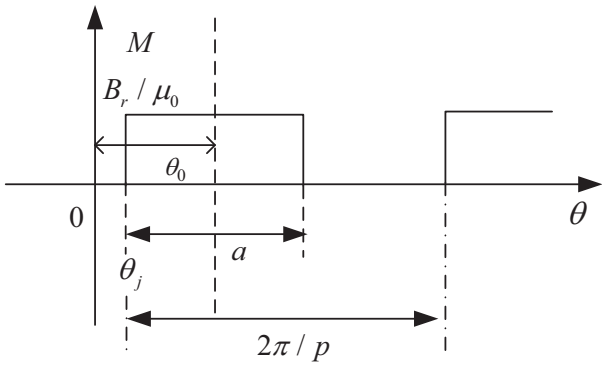

Figure 3. Radial magnetization.

where

$$a_0 = \frac{B_{\mathrm{r}}}{\mu_0} \tag{10}$$

$$\theta_j = -\frac{a}{2} + (j-1)\frac{2\pi}{p} + \theta_0, \quad j = 1, 2, \ldots, p \tag{11}$$

$$M_{\mathrm{m}} = \frac{2B_{\mathrm{r}}}{\mu_0 m\pi}[1 - (-1)^m], \quad m = 1, 2, 3 \ldots \tag{12}$$

where B_r is the radial flux density of magnets, p the number of the magnet pole pairs, a the width of magnet, θ_j the position of the jth magnet, and θ_0 can be written as $\theta_0 = \omega t$.

The field vectors $\mathbf{B}$ and $\mathbf{H}$ are written as

$$\mathbf{B_1} = \mu_0 \mathbf{H_1} \tag{13}$$

$$\mathbf{B_2} = \mu_0 \mathbf{H_2} + \mu_0 \mathbf{M} \tag{14}$$

The field intensity vectors are related to the magnetic potential functions by

$$H_{r,i} = \frac{1}{\mu}\nabla \times \mathbf{A} = \frac{1}{\mu_0}\frac{1}{r}\frac{\partial A}{\partial \theta} \tag{15}$$

$$H_{\theta,i} = \frac{1}{\mu_0}\nabla \times \mathbf{A} = -\frac{1}{\mu_0}\frac{\partial A}{\partial r} \tag{16}$$

where $i = 1$, 2 represent the air-gap subdomain and the PMs subdomain, respectively.

The continuity of the radial and tangential component of the magnetic field at $r = R_r$ leads to

$$B^j_{r,2} = B_{r,1} \quad \text{and} \quad H^j_{\theta,2} = H_{\theta,1} \tag{17}$$

else, at $r = R_r$, $\theta \in [\theta_j + a, \theta_j + \frac{2\pi}{p}]$

$$H_{\theta,1} = 0 \tag{18}$$

The boundary conditions for the jth PM subdomain are (the tangential component of the magnetic field at the sides of the PM are null) at $r = R_m$, and $\theta \in [\theta_j, \theta_j + a]$,

$$H^j_{\theta,2} = 0 \tag{19}$$

and else, at $r = R_m$ or $r = R_r$, and $\theta = \theta_j$ or $\theta = \theta_j + a$,

$$H^j_{r,2} = 0 \tag{20}$$

The regular perturbation expansion of the vector potential is proposed in the following forms [11]:

$$A_i(r, \theta, \varepsilon) = A_i^{(0)}(r, \theta) + \varepsilon A_i^{(1)}(r, \theta) + \mathrm{O}\left(\varepsilon^2\right) \tag{21}$$

So the field intensity in each subdomain is expressed as follows,

$$H_{r,i}(r,\theta,\varepsilon) = \frac{1}{\mu_0 r}\frac{\partial A_i^{(0)}(r,\theta)}{\partial \theta} + \varepsilon\frac{1}{\mu_0 r}\frac{\partial A_i^{(1)}(r,\theta)}{\partial \theta} + \mathrm{O}\left(\varepsilon^2\right) \tag{22}$$

$$H_{\theta,i}(r,\theta,\varepsilon) = -\frac{1}{\mu_0}\frac{\partial A_i^{(0)}(r,\theta)}{\partial r} - \varepsilon\frac{1}{\mu_0}\frac{\partial A_i^{(1)}(r,\theta)}{\partial r} + \mathrm{O}\left(\varepsilon^2\right) \tag{23}$$

Then groups of the governing equations and the corresponding boundary condition are derived. The zero-order governing equations are

$$\frac{\partial^2 A_1^{(0)}}{\partial r^2} + \frac{1}{r}\frac{\partial A_1^{(0)}}{\partial r} + \frac{1}{r^2}\frac{\partial^2 A_1^{(0)}}{\partial \theta^2} = 0 \tag{24}$$

$$\frac{\partial^2 A_2^{(0)}}{\partial r^2} + \frac{1}{r}\frac{\partial A_2^{(0)}}{\partial r} + \frac{1}{r^2}\frac{\partial^2 A_2^{(0)}}{\partial \theta^2} = -\mu_0 \nabla \times \mathbf{M} \tag{25}$$

The first-order governing equations are

$$\frac{\partial^2 A_1^{(1)}}{\partial r^2} + \frac{1}{r}\frac{\partial A_1^{(1)}}{\partial r} + \frac{1}{r^2}\frac{\partial^2 A_1^{(1)}}{\partial \theta^2} = 0 \tag{26}$$

$$\frac{\partial^2 A_2^{(1)}}{\partial r^2} + \frac{1}{r}\frac{\partial A_2^{(1)}}{\partial r} + \frac{1}{r^2}\frac{\partial^2 A_2^{(1)}}{\partial \theta^2} = 0 \tag{27}$$

The zero-order boundary conditions are

$$-\frac{1}{\mu_0}\frac{\partial A_1^{(0)}(r,\theta)}{\partial r}\bigg|_{r=R_s} = 0 \quad \text{and} \quad -\frac{1}{\mu_0}\frac{\partial A_2^{(0)}(r,\theta)}{\partial r}\bigg|_{r=R_m} = 0 \tag{28}$$

$$-\frac{1}{\mu_0}\frac{\partial A_1^{(0)}(r,\theta)}{\partial r} = 0, \quad r = R_r \quad \text{and} \quad \theta \in \left[\theta_j + a, \theta_j + \frac{2\pi}{p}\right] \tag{29}$$

$$-\frac{1}{\mu_0}\frac{\partial A_1^{(0)}(r,\theta)}{\partial r} = -\frac{1}{\mu_0}\frac{\partial A_2^{(0)}(r,\theta)}{\partial r} \quad r = R_r \quad \text{and} \quad \theta \in [\theta_j, \theta_j + a] \tag{30}$$

$$\frac{1}{r}\frac{\partial A_1^{(0)}(r,\theta)}{\partial \theta} = \frac{1}{r}\frac{\partial A_2^{(0)}(r,\theta)}{\partial \theta}, \quad r = R_r \quad \text{and} \quad \theta \in [\theta_j, \theta_j + a] \tag{31}$$

Similarly, the first-order boundary conditions are the same as the zero-order boundary conditions. It is no longer listed here.

2.2. The Zero-Order Solution

The general solution of the zero-order for the vector potential distribution in the air-gap subdomain and the PMs subdomain are obtained,

$$A_1^{(0)}(r,\theta) = \sum_{n=1,2,3\ldots}^{\infty}\left[\left(A_n^{(0)} r^{np} + B_n^{(0)} r^{-np}\right)\cos np\theta + \left(C_n^{(0)} r^{np} + D_n^{(0)} r^{-np}\right)\sin np\theta\right] \tag{32}$$

$$A_2^{j(0)}(r,\theta) = \sum_{m=1}^{\infty}\left[A_m^{j(0)} r^{m\pi/a} + B_m^{j(0)} r^{-m\pi/a} + \mu_0 M_m r\frac{m\pi/a}{1-(m\pi/a)^2}\right]\cos\frac{m\pi}{a}(\theta - \theta_j) \tag{33}$$

the constants $A_n^{(0)} - D_n^{(0)}$, $A_m^{j(0)}, B_m^{j(0)}$ are determined by the zero-order boundary conditions. In order to solve the boundary conditions, these constants are determined using a Fourier series expansion of the air-gap magnetic vector potentials.

Once these constants are obtained, the zero-order flux density distribution in the air-gap subdomain is:

$$B_{r,1}^{(0)} = -\sum_{n=1,2,3\ldots}^{\infty}\left[\left(A_n^{(0)}r^{np-1}+B_n^{(0)}r^{-np-1}\right)np\sin np\theta-\left(C_n^{(0)}r^{np-1}+D_n^{(0)}r^{-np-1}\right)np\cos np\theta\right] \quad (34)$$

$$B_{\theta,1}^{(0)} = -\sum_{n=1,2,3\ldots}^{\infty}\left[np\left(A_n^{(0)}r^{np-1}-B_n^{(0)}r^{-np-1}\right)\cos np\theta\right] \quad (35)$$

2.3. The First-Order Solution

The general solution of the first-order for the vector potential distribution in the air-gap subdomain and the PMs subdomain are presented as following,

$$\begin{aligned}A_1^{(1)}(r,\theta) = &\sum_{n=1,2,3\ldots}^{\infty}\left\{\begin{array}{l}\left(A_n^{(1)}r^{np-1}+B_n^{(1)}r^{-np+1}\right)\cos[(np-1)\theta]\\+\left(C_n^{(1)}r^{np-1}+D_n^{(1)}r^{-np+1}\right)\sin[(np-1)\theta]\\+\left(E_n^{(1)}r^{np+1}+F_n^{(1)}r^{-np-1}\right)\cos[(np+1)\theta]\\+\left(G_n^{(1)}r^{np+1}+H_n^{(1)}r^{-np-1}\right)\sin[(np+1)\theta]\end{array}\right\}\\&+\sum_{n=1,2,3\ldots}^{\infty}\left\{\begin{array}{l}\left(P_n^{(1)}r^{np-2}+Q_n^{(1)}r^{-np+2}\right)\cos[(np-2)\theta]\\+\left(L_n^{(1)}r^{np-2}+S_n^{(1)}r^{-np+2}\right)\sin[(np-2)\theta]\\+\left(T_n^{(1)}r^{np+2}+U_n^{(1)}r^{-np-2}\right)\cos[(np+2)\theta]\\+\left(V_n^{(1)}r^{np+2}+W_n^{(1)}r^{-np-2}\right)\sin[(np+2)\theta]\end{array}\right\}\\&+\sum_{n=1,2,3\ldots}^{\infty}\left\{\begin{array}{l}\left(X_n^{(1)}r^{np}+Y_n^{(1)}r^{-np}\right)\cos[np\theta]\\+\left(Z_n^{(1)}r^{np}+M_n^{(1)}r^{-np}\right)\sin[np\theta]\end{array}\right\}\\&+\left[\left(AA_n^{(1)}r^{1}+BB_n^{(1)}r^{-1}\right)\cos\theta+\left(CC_n^{(1)}r^{(1)}+DD_n^{(1)}r^{-1}\right)\sin\theta\right]\end{aligned} \quad (36)$$

$$A_2^{j(1)}(r,\theta) = \sum_{m=1,2,3\ldots}^{\infty}\left(A_m^{j(1)}r^{m\pi/a}+B_m^{j(1)}r^{-m\pi/a}\right)\cos\left[\frac{m\pi}{a}(\theta-\theta_j)\right] \quad (37)$$

The constants $A_n^{(1)}-M_n^{(1)}$, $AA_n^{(1)}-DD_n^{(1)}$, $A_m^{j(1)}, B_m^{j(1)}$ are determined by the first-order boundary conditions. In order to solve the boundary conditions, these constants are determined using a Fourier series expansion of the air-gap magnetic vector potentials.

Once these constants are obtained, the first-order flux density distribution in the air-gap subdomain is:

$$\begin{aligned}B_{r,1}^{(1)}(r,\theta) = \sum_{n=1,3,5\ldots}^{\infty}&\left\{\begin{array}{l}-(np-1)\left(A_n^{(1)}r^{np-2}+B_n^{(1)}r^{-np}\right)\sin[(np-1)\theta]\\+(np-1)\left(C_n^{(1)}r^{np-2}+D_n^{(1)}r^{-np}\right)\cos[(np-1)\theta]\\-(np+1)\left(E_n^{(1)}r^{np}+F_n^{(1)}r^{-np-2}\right)\sin[(np+1)\theta]\\+(np+1)\left(G_n^{(1)}r^{np}+H_n^{(1)}r^{-np-2}\right)\cos[(np+1)\theta]\end{array}\right\}\end{aligned}$$

$$
\begin{aligned}
&\left\{-(np-2)\left(P_n^{(1)}r^{np-3}+Q_n^{(1)}r^{-np+1}\right)\sin[(np-2)\theta]\right.\\
&+(np-2)\left(L_n^{(1)}r^{np-3}+S_n^{(1)}r^{-np+1}\right)\cos[(np-2)\theta]\\
+\sum_{n=1,2,3\ldots}^{\infty}&-(np+2)\left(T_n^{(1)}r^{np+1}+U_n^{(1)}r^{-np-3}\right)\sin[(np+2)\theta]\\
&\left.+(np+2)\left(V_n^{(1)}r^{np+1}+W_n^{(1)}r^{-np-3}\right)\cos[(np+2)\theta]\right\}\\
+\sum_{n=1,2,3\ldots}^{\infty}&\left\{-np\left(X_n^{(1)}r^{np-1}+Y_n^{(1)}r^{-np-1}\right)\sin[np\theta]\right.\\
&\left.+np\left(Z_n^{(1)}r^{np-1}+M_n^{(1)}r^{-np-1}\right)\cos[np\theta]\right\}\\
&+\left[-\left(AA_n^{(1)}+BB_n^{(1)}r^{-2}\right)\sin\theta+\left(CC_n^{(1)}+DD_n^{(1)}r^{-2}\right)\cos\theta\right] \qquad (38)
\end{aligned}
$$

$$
\begin{aligned}
B_{\theta,1}^{(1)}(r,\theta) \;=\; &\left\{(np-1)\left(A_n^{(1)}r^{np-2}-B_n^{(1)}r^{-np}\right)\cos[(np-1)\theta]\right.\\
&+(np-1)\left(C_n^{(1)}r^{np-2}-D_n^{(1)}r^{-np}\right)\sin[(np-1)\theta]\\
\sum_{n=1,2,3\ldots}^{\infty}&+(np+1)\left(E_n^{(1)}r^{np}-F_n^{(1)}r^{-np-2}\right)\cos[(np+1)\theta]\\
&\left.+(np+1)\left(G_n^{(1)}r^{np}-H_n^{(1)}r^{-np-2}\right)\sin[(np+1)\theta]\right\}\\
&\left\{(np-2)\left(P_n^{(1)}r^{np-3}-Q_n^{(1)}r^{-np+1}\right)\cos[(np-2)\theta]\right.\\
&+(np-2)\left(L_n^{(1)}r^{np-3}-S_n^{(1)}r^{-np+1}\right)\sin[(np-2)\theta]\\
-\sum_{n=1,2,3\ldots}^{\infty}&+(np+2)\left(T_n^{(1)}r^{np+1}-U_n^{(1)}r^{-np-3}\right)\cos[(np+2)\theta]\\
&\left.+(np+2)\left(V_n^{(1)}r^{np+1}-W_n^{(1)}r^{-np-3}\right)\sin[(np+2)\theta]\right\}\\
-\sum_{n=1,2,3\ldots}^{\infty}&\left\{np\left(X_n^{(1)}r^{np-1}-Y_n^{(1)}r^{-np-1}\right)\cos[np\theta]\right.\\
&\left.+np\left(Z_n^{(1)}r^{np-1}-M_n^{(1)}r^{-np-1}\right)\sin[np\theta]\right\}\\
&-\left[\left(AA_n^{(1)}-BB_n^{(1)}r^{-2}\right)\cos\theta+\left(CC_n^{(1)}-DD_n^{(1)}r^{-2}\right)\sin\theta\right] \qquad (39)
\end{aligned}
$$

2.4. Magnetic Field Solution of Air-gap

Based on Eqs. (36), (37), (38), and (39), the flux density distribution in the air-gap subdomain can be easily obtained:

$$B_{r,1}(r,\theta,\varepsilon) \;=\; B_{r,1}^{(0)}(r,\theta)+\varepsilon B_{r,1}^{(1)}(r,\theta) \qquad (40)$$

$$B_{\theta,1}(r,\theta,\varepsilon) \;=\; B_{\theta,1}^{(0)}(r,\theta)+\varepsilon B_{\theta,1}^{(1)}(r,\theta) \qquad (41)$$

Note that the original unperturbed flux density distribution can be easily derived when $\varepsilon = 0$.

3. APPLICATION EXAMPLE

In order to validate the proposed model, the analytical results have been compared with 2-D finite element simulations obtained using *ANSYS* software. In the finite-element analysis, the surfaces of the rotors and stator yokes as well as those of the ferromagnetic pole-pieces have been modeled by homogeneous Neumann boundary conditions as in the analytical study. The mesh in the air-gap has been refined until convergent results are obtained. In this paper, the relative permeability of the stator/rotor iron is finite, i.e., $\mu_r = 2000$. Because of the eccentricity, the finite element model needs

to be meshed when the rotor position or the eccentricity parameter changes. The FEM may not be suitable for solving eccentricity problem of motor. The solutions of this paper are presented for the case of $n_{\max} = 80$ and $m_{\max} = 40$.

The geometrical parameters given in Table 1 are considered in the simulation studies.

Table 1. Parameters of the model.

Symbol	Quantity	Value
R_s	Inner radius of the stator yoke	31.8 mm
R_r	outer radius of the rotor yoke	30.9 mm
R_m	Inner radius of the PM	24.9 mm
h_m	thickness of PM	6 mm
a	Width of PM	45°
g	Air-gap length	0.9 mm
B_r	Remanence of the PMs	1.12 T
p	Number of pole-pairs	4
L_{ef}	Axial length	48 mm

Figure 4 shows the magnetic flux lines for the proposed model excited by PMs.

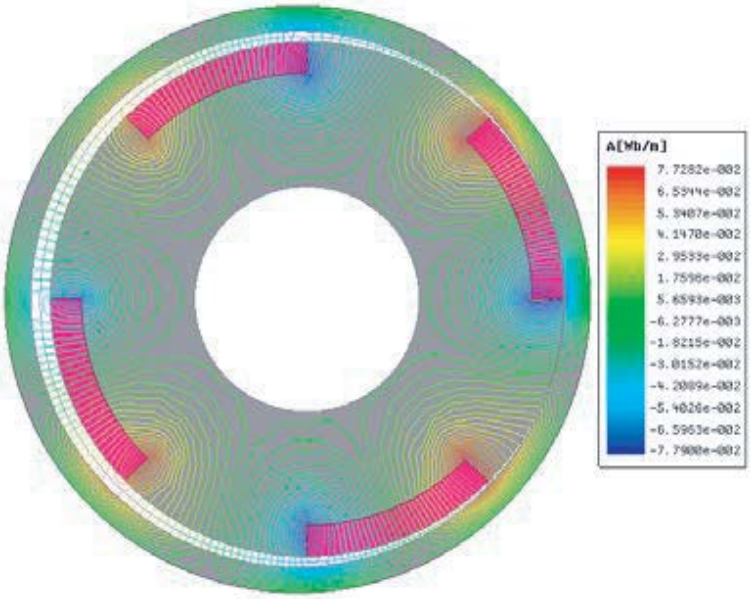

Figure 4. Magnetic flux line distribution for the studied motor.

Figure 5 shows the radial and tangential flux densities on a circle of the air-gap, and there is no rotor eccentricity at an instant of $\omega t = 0°$. A good agreement is noticed between the analytical and numerical computations.

Figure 6 shows the flux density distribution in the air-gap for the case of $d = 0.2$ mm at an instant of $\omega t = 30°$. Again, the distributions show good agreement in two methods.

The analytical and finite element results of the eccentric force at different eccentricities are listed in Table 2, in which the rotor is at $\omega t = 0°$.

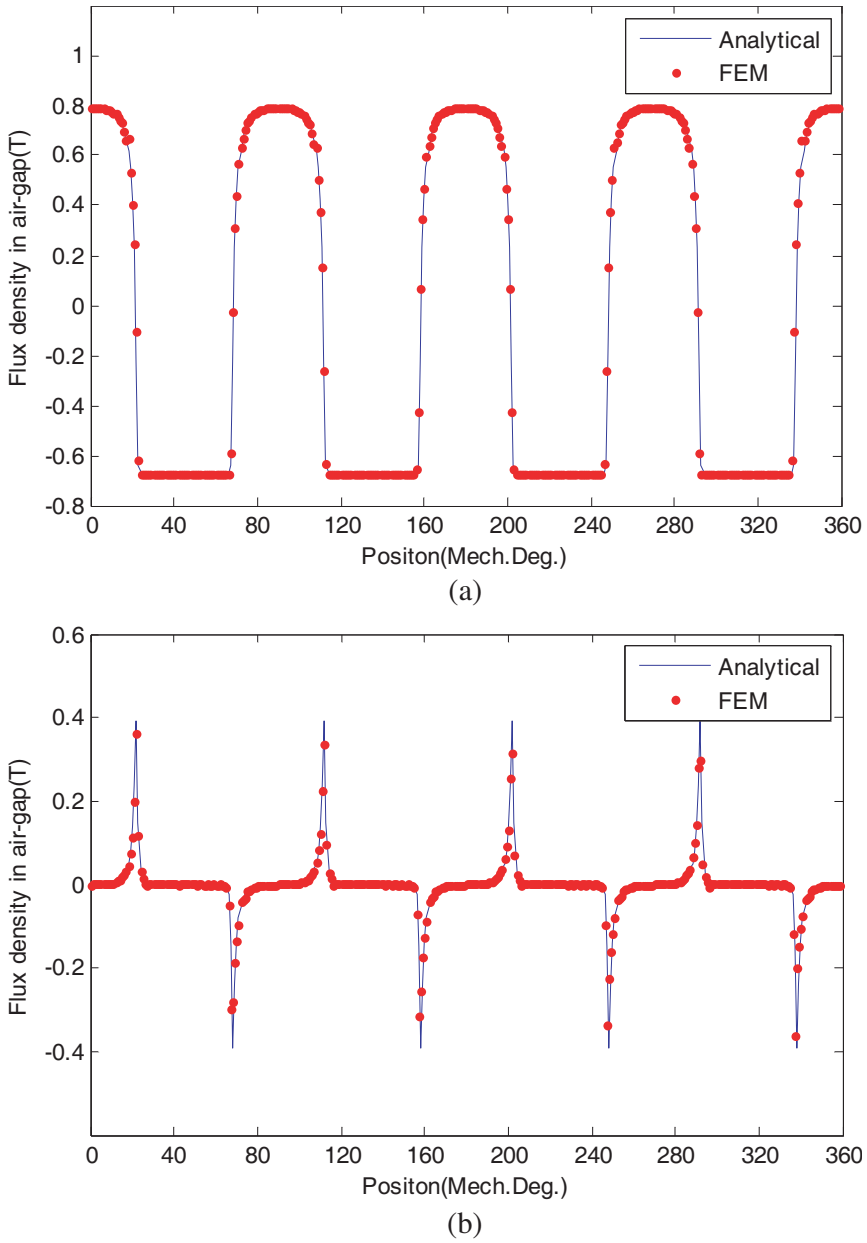

Figure 5. Flux density distribution in the air-gap predicted by analytical and FE at $r = R_r + g/2$ and $\omega t = 0°$ with no rotor eccentricity. (a) Radial component. (b) Tangential component.

Table 2. Comparisons between analytical solution and FE solution of eccentric force.

d/mm	Eccentric force/N		Relative error/(%)
	Analytical	FEM	
0.018	10.167	10.186	0.19
0.045	50.842	50.982	0.27
0.09	101.72	100.89	0.82
0.18	203.565	202.35	0.64
0.27	305.372	307.94	0.83

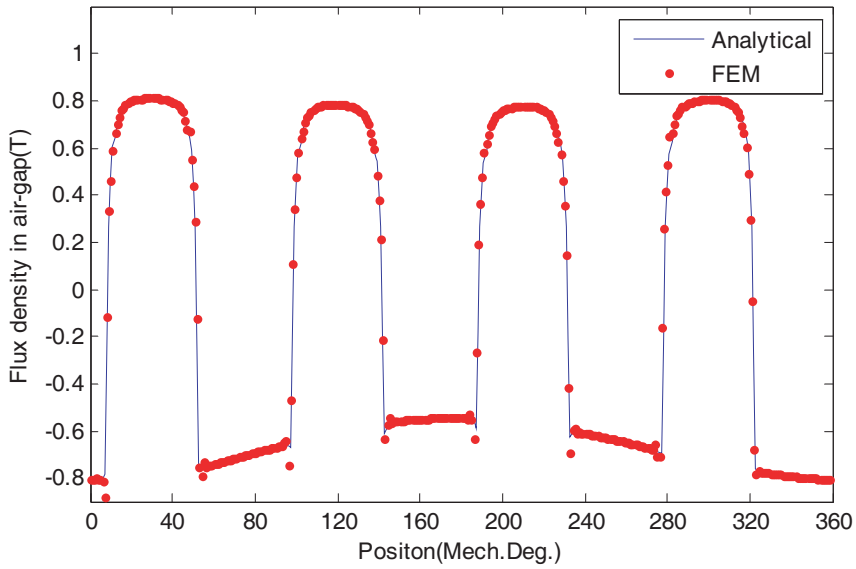

(a)

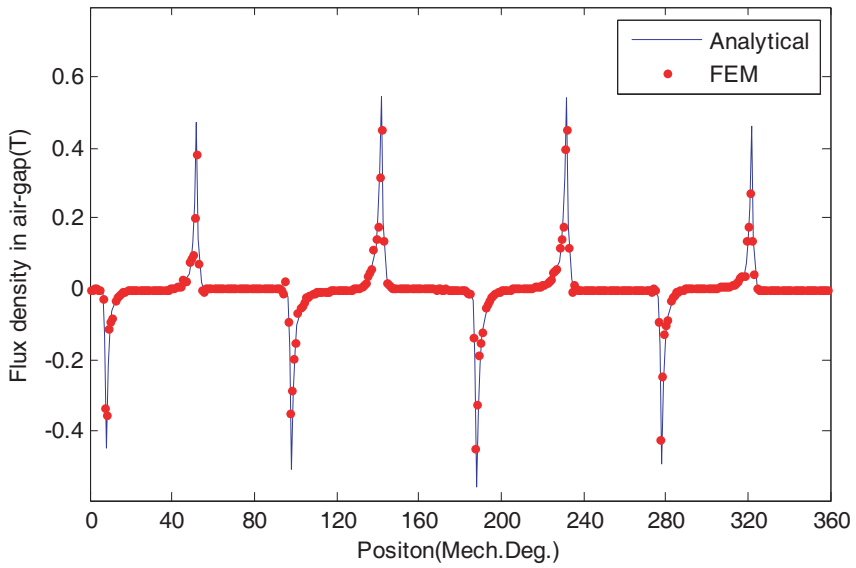

(b)

Figure 6. Flux density distribution in the air-gap predicted by analytical and FE at $r = R_r + (g-d)/2$ and $\omega t = 30°$. (a) Radial component. (b) Tangential component.

4. CONCLUSION

In this paper, an exact 2-D analytical method for predicting the magnetic field distribution in a consequent-pole bearingless motor considering the rotor eccentricity has been presented. The proposed method is utilized to formulate the governing equations and boundary conditions. Due to consequent-pole, the general solution of the first-order for the vector potential distribution in the air-gap is presented considering first harmonic. Flux density computation is in close agreement with those of FE predictions. The results show that this method is sufficiently accurate for the prediction of the magnetic field distribution of consequent-pole bearingless motor. This method is easy to modify and can conveniently calculate the magnetic field distribution of the motor under various rotor positions and eccentric parameters. It will also help to develop motors with better design.

ACKNOWLEDGMENT

This work was supported by the National Natural Science Foundation of China (Project No. 51707072), China Postdoctoral Science Foundation (Project No. 2018M632855).

REFERENCES

1. Chiba, A., D. T. Power, and M. A. Rahman, "Characteristics of a bearingless induction motor," *IEEE Trans. Magn.*, Vol. 27, No. 6, 5199–5201, 1991.
2. Ooshima, M., A. Chiba, T. Fukao, and M. A. Rahman, "Design and analysis of permanent magnet-type bearingless motors," *IEEE Trans. Ind. Electro.*, Vol. 43, No. 2, 292–299, 1996.
3. Ooshima, M., S. Miyazawa, and A. Chiba, "A rotor design of a permanent magnet-type bearingless motor considering demagnetization," *IEEE Proc., Power Conversion Conf.*, 655–660, Nagaoka, 1997.
4. Qiu, Z. J., "Fundamental research on permanent-magnet type bearingless motors," Nanjing Univ. Aeron and Astron., Nanjing, 2010.
5. Oshima, M., S. Miyazawa, and T. Deido, "Characteristics of a permanent magnet type bearingless motor," *IEEE Trans. Ind. Appl.*, Vol. 32, No. 2, 363–370, 1996.
6. Qiu, Z. J., Z. Q. Deng, X. L. Wang, and L. K. Meng, "The principle and implementation of a new-type consequent-pole bearingless permanent magnet motor," *Proc. of the CSEE*, Vol. 27, No. 33, 01–05, 2007.
7. Kim, U. and D. K. Lieu, "Magnetic field calculation in permanent magnet motors with rotor eccentricity: Without slotting effect," *IEEE Trans. Magn.*, Vol. 34, No. 4, 2243–2252, Jul. 1998.
8. Kim, U. and D. K. Lieu, "Magnetic field calculation in permanent magnet motors with rotor eccentricity: With slotting effect considered," *IEEE Trans. Magn.*, Vol. 34, No. 4, 2253–2266, Jul. 1998.
9. Kim, U. and D. K. Lieu, "Effects of magnetically induced vibration force in brushless permanent-magnet motors," *IEEE Trans. Magn.*, Vol. 41, No. 6, 2164–2172, Jun. 2005.
10. Rahideh, A. and T. Korakianitis, "Analytical open-circuit magnetic field distribution of slotless brushless permanent magnet machines with rotor eccentricity," *IEEE Trans. Magn.*, Vol. 47, No. 12, 4791–4808, 2011.
11. Fu, J. J. and C. S. Zhu, "Subdomain model for predicting magnetic field in slotted surface mounted permanent magnet machines with rotor eccentricity," *IEEE Trans. Magn.*, Vol. 48, No. 5, 1906–1917, 2012.
12. Li, C., Y. J. Zhang, and Z. J. Qiu, "Exact analytical model for the no-load air-gap magnetic field calculation in consequent-pole permanent magnet bearingless motor," *Trans. China Electro. Society*, Vol. 27, No. 11, 01–05, 2012.
13. Fu, W. B., H. He, and Z. K. Chen, "Mode analyses of quasi-rectangular waveguides by using PMOBG," *Journal of Jishou University*, Vol. 24, No. 4, 43–47, 2003.
14. Lubin, T., S. Mezani, and A. Rezzoug, "Exact analytical method for magnetic field computation in the air gap of cylindrical electrical machines considering slotting effects," *IEEE Trans. Magn.*, Vol. 46, No. 4, 1092–1099, Apr. 2010.